Title

Relationship between spatially heterogeneous reaction dynamics and photochemical kinetics in single crystals of anthracene derivatives.

Journal

Chemical Science, 15(33)

ISSN

2041-6520

Authors

Kataoka, Sogo

Kitagawa, Daichi

Sotome, Hikaru

et al.

Publication Date

2024-08-22

DOI

10.1039/d4sc03060e

Peer reviewed

Chemical Science

ROYAL SOCIETY OF CHEMISTRY

EDGE ARTICLE

Cite this: *Chem. Sci.*, 2024, **15**, 13421

All publication charges for this article have been paid for by the Royal Society of Chemistry

Received 10th May 2024
Accepted 7th July 2024

DOI: 10.1039/d4sc03060e

rsc.li/chemical-science

Relationship between spatially heterogeneous reaction dynamics and photochemical kinetics in single crystals of anthracene derivatives†

Sogo Kataoka,[a] Daichi Kitagawa, *[a] Hikaru Sotome, [b] Syoji Ito, [b] Hiroshi Miyasaka, [b] Christopher J. Bardeen *[c] and Seiya Kobatake *[a]

Understanding physicochemical property changes based on reaction kinetics is required to design materials exhibiting desired functions at arbitrary timings. In this work, we investigated the photodimerization of anthracene derivatives in single crystals. Single crystals of 9-cyanoanthracene (**9CA**) and 9-anthraldehyde (**9AA**) exhibited reaction front propagation on the optical length scale, while 9-methylanthracene and 9-acetylanthracene crystals underwent spatially homogeneous conversion. Moreover, the sigmoidal behavior in the absorbance change associated with the reaction was much pronounced in the case of **9CA** and **9AA** and correlated with the observation of heterogeneous reaction progress. A kinetic analysis based on the Finke–Watzky model showed that the effective quantum yield of the photochemical reaction changes by more than an order of magnitude during the course of the reaction in **9CA** and **9AA**. Both the reaction front propagation and nonlinear kinetic behavior could be rationalized in terms of the difference in the cooperativity of the reactions. We propose a plausible mechanism for the heterogeneous reaction progress in single crystals that depends on the magnitude of the conformational change required for reaction. Our results provide useful information to understand the connection between photochemical reaction progress in the crystalline phase and the dynamic changes in the physicochemical properties.

Introduction

In recent years, stimuli-responsive organic crystals that exhibit functions such as fluorescence color change,[1,2] superelasticity,[3,4] self-healing,[5–8] and gas adsorption/desorption[9] in response to external stimuli have been attracting attention as next-generation functional materials.[10,11] Changes in the physical properties of stimuli-responsive crystalline materials are generally brought about by changes in the molecular structure or crystal packing.[12,13] These structural changes can be accurately determined by single-crystal X-ray diffraction (SCXRD) measurements, which provide molecular-level insight into why changes in physicochemical property occur.[14–17] However, this method only captures the "static" state before and after the structural change and it is generally difficult to capture the "dynamic" changes. In order to design stimuli-responsive organic crystals that exhibit desired functions at arbitrary timings, it is necessary to understand how reaction dynamics in crystals give rise to changes in physical properties.

Reactions in the crystalline state often show different behavior from those in solution.[18–21] This is because the molecule in the crystalline state is surrounded by many other molecules and intermolecular interactions with its neighbors exert a strong influence on its dynamics. This situation is significantly different from the solution state where molecules evolve independently. For the purposes of this paper, a cooperative process is one in which the reactant–product interactions are strong enough to give rise to a measurable deviation from the exponential behavior observed for molecules reacting independently in dilute solution.[22] As an example, in the case of the [2 + 2] photodimerization reaction of cinnamic acid crystals, the reaction does not progress much immediately after the start of photoirradiation, but once the reaction starts, the reaction progresses rapidly.[23] This is due to the cooperative effects that cause reactant molecules around the products to become more reactive. In these cases, the plot of the conversion ratio from the reactant to the product relative to the irradiation time shows a sigmoidal curve.[23] To correctly analyze changes in solid-state properties, kinetic analysis of reactions using theoretical

[a]*Department of Chemistry and Bioengineering, Graduate School of Engineering, Osaka Metropolitan University, 3-3-138 Sugimoto, Sumiyoshi-ku, Osaka , 558-8585, Japan. E-mail: kitagawa@omu.ac.jp; kobatake@omu.ac.jp*

[b]*Division of Frontier Materials Science and Center for Promotion of Advanced Interdisciplinary Research, Graduate School of Engineering Science, Osaka University, 1-3 Machikaneyama-cho, Toyonaka, Osaka 560-8531, Japan*

[c]*Department of Chemistry, University of California, Riverside, 501 Big Springs Road, Riverside, CA 92521, USA. E-mail: christob@ucr.edu*

† Electronic supplementary information (ESI) available: Measurements of crystal thickness and powder X-ray diffraction, molecular packing diagrams in crystals, the results of fittings, and movies. See DOI: https://doi.org/10.1039/d4sc03060e

models incorporating cooperative reaction processes is essential.

We recently investigated the photochemical reaction kinetics of 9-methylanthracene (**9MA**) in the crystalline phase where it undergoes photodimerization.[24] Interestingly, the photochemical kinetics of **9MA** in single crystals were close to exponential while those for polycrystalline samples had a pronounced sigmoidal behavior, which is presumably due to the difference in crystal defects. The extended Finke–Watzky (FW) model that we have developed reproduced both regimes in terms of an effective quantum yield that depends on reaction progress. This approach provides a way to quantify the cooperativity of the photochemical reactions in the crystalline state. Furthermore, in the course of study on the photochemical reaction dynamics in organic molecular single crystals, we found that the photochemical reaction of 2,5-distyrylpyrazine (DSP) in single crystals proceeds from the edge to the center of the crystal.[25] Namely, the photochemical reaction of DSP proceeds heterogeneously on length scales that can be resolved by optical microscopy, typically on the order of 1 micron, in contrast to photochemical reactions in single crystals that proceed homogeneously on such optical length scales. Heterogeneous reaction dynamics have been observed in the context of thermal polymorphic transitions,[26–29] but have only recently been demonstrated for photochemical reactions. However, it remains unclear what factors cause a photochemical reaction to be heterogeneous on the optical length scale.

The observation of cooperative reaction kinetics (in the form of sigmoidal time behavior) and spatial reaction front propagation raises the question of whether these two phenomena are related. To address this issue, in this work we measure both the photochemical kinetics on the molecular scale and the progress of the photochemical reaction on the optical length scale for single crystals composed of anthracene derivatives. **9MA**, 9-acetylanthracene (**9AcA**), 9-cyanoanthracene (**9CA**), and 9-anthraldehyde (**9AA**) are selected as the candidates (Fig. 1). The spatial progress of the photochemical reaction, observed under crossed Nicols using a polarized optical microscope, shows different behaviors depending on the compounds. The photochemical kinetic analysis for the change in the absorbance using the extended FW model reveals that the cooperative effect also depends greatly on the compounds. We find that the magnitude of the molecular conformational change associated with the photochemical reaction in crystals strongly correlates with both cooperative reaction kinetics and the observation of heterogeneous reaction dynamics on the optical length scale. The observation that different crystal packing motifs can give rise to very different kinetic behaviors provides a dramatic example of a novel solid-state structure–function relationship.

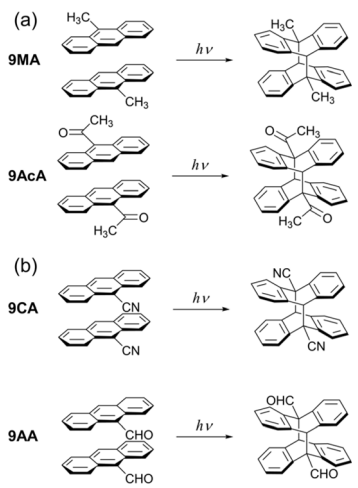

Fig. 1 Photodimerization reaction of 9MA, 9AcA, 9CA, and 9AA in the crystalline phase. (a) The photodimerization proceeds in a topotactic manner. (b) The photodimerization involves large molecular conformational changes.

Experimental

Materials

9MA and **9AA** were purchased from TCI and used as received. **9AcA** and **9CA** were purchased from Sigma-Aldrich and used as received.

Preparation of single crystals

The single crystals of **9MA**, **9AcA**, **9CA**, and **9AA** were prepared as follows. As for **9MA** and **9AcA**, the compounds were dissolved in tetrahydrofuran (THF). Then, the solution was dropped onto water on a slide glass. After evaporation of THF and water in the dark, single crystals were obtained. In the case of **9CA** and **9AA**, the compounds were dissolved in THF. Then, the solution was mixed with water in a Petri dish. Then, it was left undisturbed in the dark, resulting in the crystallization due to the evaporation of THF. The face indices of the samples were determined by powder X-ray diffraction (PXRD) measurement using a Rigaku MiniFlex 600 diffractometer employing CuK_α radiation (λ = 1.54184 Å).

Microscopic observation of crystals

Optical microphotographs of interference color under crossed Nicols were obtained using a Nikon ECLIPSE E600POL or an Olympus BX53-P polarizing optical microscope equipped with a video camera system. Polarized absorption spectra were measured using the polarizing optical microscope equipped with a EBA JAPAN NH-2DK hyperspectral camera. The hyperspectral camera is capable of acquiring spectral information for each pixel of the captured image, but we used information averaged over about 2 μm^2 to reduce errors. Light irradiation of the crystals was carried out using a super high-pressure mercury lamp (100 W; bandpass filter (405 nm light excitation)) attached to the polarizing optical microscope. The 405 nm light was applied to the entire crystal with uniform intensity. The power of the light irradiation was measured using a THORLABS PM160 optical power meter. The crystal thickness was measured using a KEYENCE VK-8700 laser scanning microscope. The interference color change accompanying the birefringence change was observed under crossed Nicols.

Results and discussion

Progress of the photochemical reaction on the optical length scale

First, the single crystals of **9MA**, **9AcA**, **9CA**, and **9AA** were prepared by the procedures described in the Experimental section. The crystal thickness of the samples was in the range 1.0–3.0 μm as shown in Fig. S1.† Then, PXRD measurements were performed to characterize the molecular orientation of the single crystals (Fig. S2†). From the comparison of the experimental peaks with the calculated patterns using the CIF files (CCDC No. 1209376, 1139795, 1127855, 1103100) obtained by SCXRD measurements,[30–33] the observed faces of the single crystals were determined to be the (100), (10-1), (120), and (002) faces for **9MA**, **9AcA**, **9CA**, and **9AA**, respectively (Fig. S3†).

Next, we observed the single crystals of **9MA**, **9AcA**, **9CA**, and **9AA** under crossed Nicols using a polarized microscope (Fig. 2 and Movies S1–S4†). Before photoirradiation, the single crystals exhibited an interference color originating from the birefringence. The birefringence change is very sensitive to the photochemical reactions and proportional to the fractional conversion to the photoproducts.[34] Therefore, observation of birefringence change during the reaction provides information about the spatial progress of the photochemical reaction.[24,34,35] Upon irradiation with 405 nm light, the interference color changed as the photodimerization reaction proceeds. Interestingly, we found that there are two types of reaction progress. In the case of **9MA** and **9AcA**, the interference color changed uniformly across the entire crystal, *i.e.* homogeneously on the optical length scale. In contrast, the change in the interference color started from the edge to the center of the crystal in the case of **9CA** and **9AA**, indicating that the photodimerization reaction proceeded heterogeneously on the optical length scale. Note that the interference color of the single crystals of **9CA** and **9AA** became dark after completion of the photoreaction due to the loss of the crystallinity. In addition, we investigated the change in fluorescence intensity during photodimerization. In the case of **9MA** and **9AcA**, the fluorescence intensity decrease was spatially homogeneous (Movies S5 and S6†), while for **9CA** and **9AA** there was a clear phase front (Movies S7 and S8†). For both sets of molecules, the fluorescence evolution mirrored the change in birefringence. Thus, it was revealed that the progress of the photochemical reaction on the optical length scale depends on the compounds.

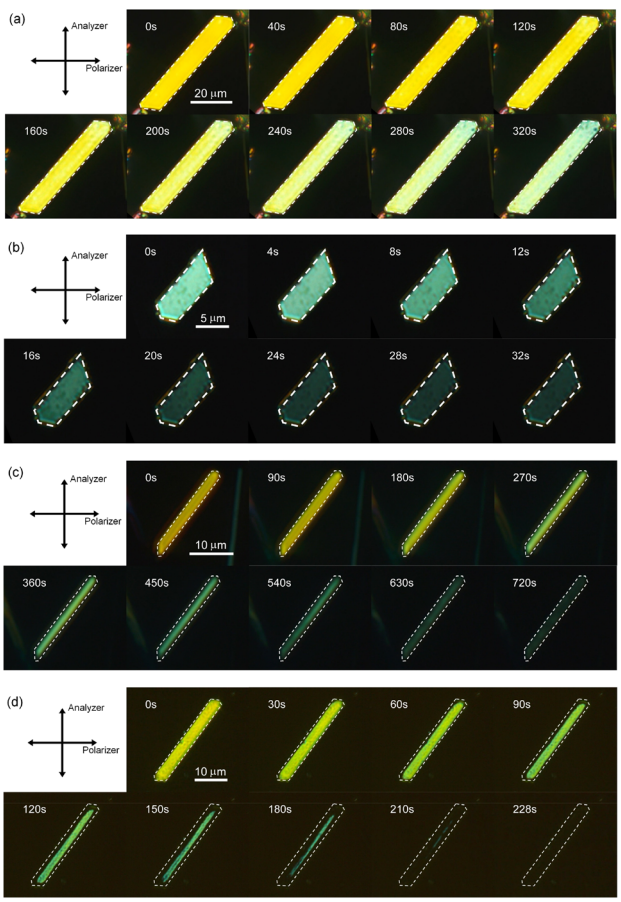

Fig. 2 Interference color change of (a) **9MA**, (b) **9AcA**, (c) **9CA**, and (d) **9AA** single crystals observed under crossed Nicols upon irradiation with 405 nm light.

Photochemical reaction kinetics on the molecular scale

The absorbance changes due to the photodimerization reaction in single crystals of **9MA**, **9AcA**, **9CA**, and **9AA** were investigated using a hyperspectral camera that allows us to measure the absorbance changes at different spots in a single crystal. In all samples, the averaged absorbance across single crystals decreased as the photodimerization reaction proceeded (Fig. 3a–d). This is because the dimerization reaction destroys the conjugation of the anthracene ring.[36] Fig. 3e–h show the averaged absorbance decay profiles of **9MA**, **9AcA**, **9CA**, and **9AA** upon photoirradiation. In all cases, the decay profiles show some sigmoidal character, but those of **9CA** and **9AA** are much pronounced than those of **9MA** and **9AcA**. This suggests that the cooperative effect varies widely among the compounds.

Furthermore, the absorbance decay profiles at different spatial locations in single crystals were also different depending on the compounds. In the case of **9MA** and **9AcA**, the absorbance change for separate spots across a single crystal were almost the same (Fig. 4a and b), whereas the absorbance attenuates first at the edges of the crystal in the case of **9CA** and **9AA** (Fig. 4c and d). This agrees with the results of the observation of interference color changes described above. In this way, from the results of absorbance changes at different spots, it was also confirmed that the photochemical reaction proceeds homogeneously on the optical length scale in the single crystals of **9MA** and **9AcA** but proceeds heterogeneously in single crystals of **9CA** and **9AA**.

To quantitatively analyze the absorbance decay profiles, we first applied the commonly used JMAK equation (Johnson–Mehl–Avrami–Kolmogorov)[37–40] (eqn (1))

$$f = 1 - e^{-(kt)^n} \quad (1)$$

where f is the conversion ratio, k is the reaction rate constant, t is the irradiation time, and n is the Avrami exponent. n takes

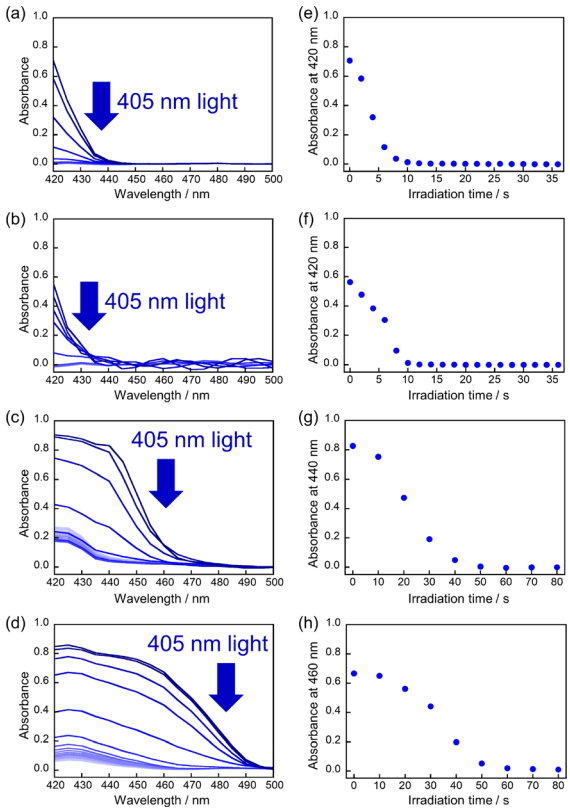

Fig. 3 Decrease in the averaged absorbance across single crystals due to the photodimerization upon irradiation with 405 nm light for (a) **9MA**, (b) **9AcA**, (c) **9CA**, and (d) **9AA**. The absorbance decay profiles *versus* irradiation time for (e) **9MA**, (f) **9AcA**, (g) **9CA**, and (h) **9AA**, showing different sigmoidal behaviors depending on the compound.

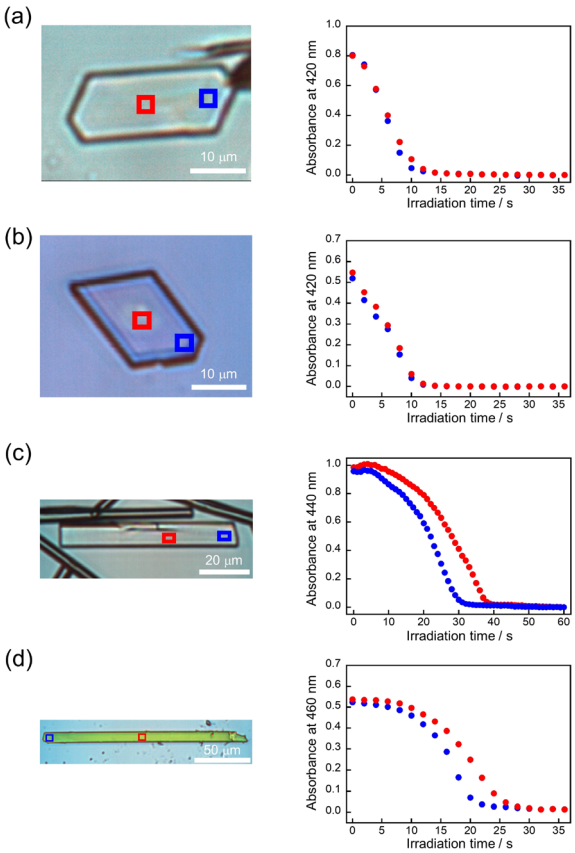

Fig. 4 Absorbance decay profiles *versus* irradiation time due to photodimerization of (a) **9MA**, (b) **9AcA**, (c) **9CA**, and (d) **9AA**. The red and blue squares in the single crystals indicate the locations where absorbance was measured and correspond to the colors of the absorbance decay profiles.

a value ranging from 0 to 4. $n = 1$ corresponds to normal exponential behavior, while $n < 1$ indicates autoinhibitory kinetics and $n > 1$ indicates autocatalytic kinetics. $n \neq 1$ is a signature of cooperative kinetics and the larger the deviation, the greater the cooperativity.

Fig. S4–S6† show the results of the fitting of the change in conversion calculated from absorbance decay profiles of **9MA**, **9AcA**, **9CA**, and **9AA** with eqn (1). Note that the averaged absorbance across single crystals was used for the fitting and the fitting was performed 3 times using different samples. The parameters used for the fitting are summarized in Table 1. Fig. S7–S9† show the results of the fitting of absorbance decay in different single crystals of **9MA**, **9AcA**, **9CA**, and **9AA**. The n value ranged from 1.6–2.0 for **9MA**, 1.8–2.2 for **9AcA**, 2.4–2.9 for **9CA**, and 2.8–3.2 for **9AA**. The value of n increased sharply for **9CA** and **9AA**. Therefore, it can be said that the single crystals of **9AA** and **9CA** have a more pronounced cooperativity than those of **9AcA** and **9MA**.

Next, to get more insights from the viewpoint of photochemistry, we applied the extended FW model that we developed previously.[41,42] The extended FW model consists of four elementary reactions if A represents the monomer pair, and B the photodimer (eqn (2a)–(2d)).

$$\mathrm{A} \xrightarrow{\sigma I} \mathrm{A}^* \tag{2a}$$

$$\mathrm{A}^* \xrightarrow{k_{ex}} \mathrm{A} \tag{2b}$$

$$\mathrm{A}^* + \mathrm{A} \xrightarrow{k_1} \mathrm{B} + \mathrm{A} \tag{2c}$$

$$\mathrm{A}^* + \mathrm{B} \xrightarrow{k_2} \mathrm{B} + \mathrm{B} \tag{2d}$$

Table 1 Summary of the constants obtained by fitting of the absorbance decay using eqn (1)

	Sample	k (s^{-1})	n
9MA	1	0.221	2.0
	2	0.156	1.6
	3	0.270	1.8
9AcA	4	0.153	2.2
	5	0.166	2.0
	6	0.146	1.8
9CA	7	0.039	2.4
	8	0.035	2.9
	9	0.048	2.8
9AA	10	0.021	3.2
	11	0.022	2.8
	12	0.026	3.2

where σ is the absorption cross section at the excitation wavelength (cm^2 per molecule), I is the monochromatic light intensity for the photoreaction (photons per cm^2 per s), k_{ex} is the relaxation rate constant of A to the ground state (s^{-1}). k_1 and k_2 are the rate constants (nm^3 per molecule per s) of the reactions that are affected by A and B, respectively. As reported in our previous work, based on these elementary reactions, we can finally obtain an equation to fit the measured Abs(t) curves:

$$\frac{\mathrm{d\ Abs}}{\mathrm{d}t} = -\frac{\sigma I_0}{\ln(10)}\left(1-10^{-\mathrm{Abs}}\right)\left(\frac{\frac{\mathrm{Abs}}{\mathrm{Abs}_0}+\beta\left(1-\frac{\mathrm{Abs}}{\mathrm{Abs}_0}\right)}{\alpha+\frac{\mathrm{Abs}}{\mathrm{Abs}_0}+\beta\left(1-\frac{\mathrm{Abs}}{\mathrm{Abs}_0}\right)}\right) \quad (3)$$

where $\alpha = k_{ex}/k_1[A]_0$, $\beta = k_2/k_1$, Abs is the monomer absorbance at the excitation wavelength, Abs_0 is the initial absorbance at the excitation wavelength, and $[A]_0$ is the initial monomer pair concentration (molecule per nm^3). Fitting the experimental data using eqn (3) yields the constants α and β. From these values, we can extract the effective quantum yields, which is a quantity interpretable from photochemistry standard concepts, using following equations,

$$\Phi_1 = \frac{k_1[A]}{k_{ex}+k_1[A]+k_2[B]} = \frac{1-f}{\alpha+1-f+\beta f} \quad (4a)$$

$$\Phi_2 = \frac{k_2[B]}{k_{ex}+k_1[A]+k_2[B]} = \frac{\beta f}{\alpha+1-f+\beta f} \quad (4b)$$

where $f = ([A]_0 - [A])/[A]_0 = [B]/[A]_0$ is the fraction of crystal converted to photodimer. Note that Φ_1 and Φ_2 depend on the dimer fraction f. The total quantum yield Φ_{1+2} related to the photoreaction can be described by,

$$\Phi_{1+2} = \Phi_1 + \Phi_2 = \frac{1-f+\beta f}{\alpha+1-f+\beta f} \quad (5)$$

Note that if $\beta = 1$, Φ_{1+2} does not depend on f. Furthermore, as reported in our previous study, the $\Phi_{1+2,f=1}/\Phi_{1+2,f=0}$ is a useful quantity to parameterize the decay shape. When the value is relatively large, the curves have a definite induction period. On the other hand, as the ratio approaches unity, the curves are closer to single exponential. Therefore, we can evaluate the cooperativity quantitatively using the value of $\Phi_{1+2,f=1}/\Phi_{1+2,f=0}$.

Fig. S7–S9† show the results of the fitting of absorbance decay profiles in single crystals of **9MA**, **9AcA**, **9CA**, and **9AA** with eqn (3). Note that the averaged absorbance across single crystals was used for the fitting and the fitting was performed 3 times using different samples. The parameters used for the fitting are summarized in Table 2. The $\Phi_{1+2,f=1}/\Phi_{1+2,f=0}$ was in the range 2.8–4.6 for **9MA**, 7.8–8.9 for **9AcA**, 30.7–41.4 for **9CA**, and 77.1–84.9 for **9AA**. Thus, the value of $\Phi_{1+2,f=1}/\Phi_{1+2,f=0}$ increased in the order of **9MA**, **9AcA**, **9CA**, and **9AA**. This agrees with the results of the fitting using JMAK equation. Note that this trend holds for any value of σ in the range 1.5×10^{-18} to 1.5×10^{-16} cm^2 per molecule, so it does not rely on the exact value of the absorption cross-section, which has some uncertainty. This analysis is more complicated than the JMAK model but provides additional parameters with clear chemical meaning. The data in Table 2 show that there is a dramatic difference between the **9MA**/**9AcA** crystals and the **9CA**/**9AA** crystals. In the latter crystals, the effective quantum yield increases by more than an order of magnitude as the reaction proceeds.

Physical origin of cooperative reaction kinetics and spatially heterogeneous photochemical reactions

All crystals studied here exhibit some degree of cooperative kinetics in which the rate speeds up as the reaction proceeds. One possible explanation for this speed up could be photothermal heating that raises the crystal temperature during the illumination period. However, these crystals are only a few microns thick and are adhered to a thick glass substrate that acts as a heat sink. If we assume a thermal diffusivity of 10^{-7} m^2 s^{-1},[43] heat transfer across the crystal thickness occurs within milliseconds. Given the reactions occur on timescales of seconds, it is unlikely that non-equilibrated thermal gradients could build up during the observation period. It is also not clear why photothermal effects would be more pronounced for **9CA** and **9AA** as compared to **9MA** and **9AcA**. However, it would be interesting for future studies to investigate how the temperature (or heat) affects the reaction rate.

To explain why the progress of the photochemical reaction on the optical length scale varies with compound, we instead focus on the molecular conformational change associated with the photodimerization reaction. In previous studies, the molecular structure and packing before and after the photodimerization reaction of **9MA**, **9AcA**, **9CA**, and **9AA** have been already reported.[44–46] In the case of **9MA** and **9AcA**, they undergo a typical topotactic photodimerization reaction maintaining the head-to-tail packing of the monomer pair (Fig. 1a). On the other hand, **9CA** and **9AA** undergo an unusual photodimerization (non-topotactic) reaction that requires a large molecular conformational change from head-to-head to head-to-tail packing (Fig. 1b).[47,48] It is not clear why the different substituents lead to different initial packing motifs, but we suspect that these motifs require large conformational changes for the **9CA** and **9AA** dimerization reactions, giving rise to their highly heterogeneous reaction kinetics.

We know that at least one **9CA**/**9AA** molecule must flip in order to adopt the head-to-tail configuration that permits the photodimerization to occur. This can happen at defect sites, or in regions where the barrier to this flipping is much lower. Both of these conditions are more likely to occur at the crystal surface. The interior of the crystal is densely packed with monomer pairs, so dimerization requiring a large structural change, like the case of **9CA** and **9AA**, is unlikely to occur. Then, the dimerization of monomer pairs on the crystal surface results in the increase of the free volume of the surrounding monomer pairs, facilitating the dimerization reaction. By a series of such reactions, the photoreaction proceeds sequentially from the edge to the center of the crystal (Fig. 5). **9MA** and **9AcA**, on the other hand, have a head-to-tail packing that positions the molecules for facile photodimerization, so reactions in the interior occur at the same rate as those at the edges, leading to a spatially homogeneous transformation.

Table 2 Summary of the constants obtained by fitting of the absorbance decay using eqn (3)[a]

	Sample	α	β	$\Phi_{1,f=0}$	$\Phi_{2,f=0}$	$\Phi_{1,f=1}$	$\Phi_{2,f=1}$	$\Phi_{1+2,f=1}/\Phi_{1+2,f=0}$
9MA[b]	1	3.5	22.7	0.224	0.0	0.0	0.868	3.9
	2	5.4	14.1	0.157	0.0	0.0	0.724	4.6
	3	2.0	25.6	0.333	0.0	0.0	0.928	2.8
9AcA[b]	4	10.1	28.6	0.0900	0.0	0.0	0.739	8.2
	5	10.0	24.7	0.0907	0.0	0.0	0.711	7.8
	6	11.5	29.0	0.0802	0.0	0.0	0.717	8.9
9CA[c]	7	5.8×10^4	41.4	1.7×10^{-5}	0.0	0.0	7.1×10^{-4}	41.4
	8	4.6×10^4	39.6	2.2×10^{-5}	0.0	0.0	8.6×10^{-4}	39.5
	9	3.5×10^4	30.7	2.9×10^{-5}	0.0	0.0	8.9×10^{-4}	30.7
9AA[d]	10	1.3×10^3	85.7	7.9×10^{-4}	0.0	0.0	6.3×10^{-2}	80.4
	11	1.2×10^3	82.3	8.3×10^{-4}	0.0	0.0	6.4×10^{-2}	77.1
	12	1.0×10^3	92.5	9.7×10^{-4}	0.0	0.0	8.2×10^{-2}	84.9

[a] σ was set to 1.5×10^{-17} cm^2 per molecule. [b] I_0 was 3.9×10^{16} photons per cm per s. [c] I_0 was 2.7×10^{19} photons per cm per s. [d] I_0 was 1.8×10^{17} photons per cm per s.

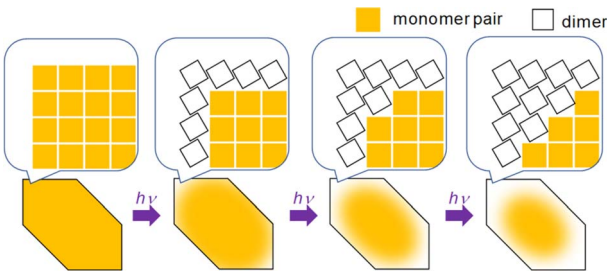

Fig. 5 Schematic illustration of the mechanism of the heterogeneous photochemical reaction on the optical length scale.

The induced defect mechanism for heterogeneous reaction dynamics can also qualitatively explain the dependence of the reaction yield on reaction progress (Table 2). If the reaction requires large rearrangements within a pristine crystal, then at the start of the reaction most of the incoming photons are "wasted" after being absorbed by molecules that cannot dimerize. Once a significant fraction has reacted and disrupted the original head-to-head lattice, molecular rotation and defects will become more widespread, and an excited molecule will be more likely to have the opportunity to dimerize. Therefore, both **9CA** and **9AA** require an induction period while disorder builds up in the crystal, which eventually increases the reaction quantum yield by a factor of 30-80. **9MA** and **9AcA**, in contrast, are already well-positioned for dimerization by the head-to-tail crystal packing, but still benefit from the reaction induced strain as the reaction proceeds. Interestingly, we found earlier that high defect densities in polycrystalline **9MA** could actually slow down the reaction and lead to more sigmoidal kinetics.[24] In that case, static structural disorder probably leads to misaligned **9MA** pairs that must reconfigure to react, similar to the ordered packing in **9CA** and **9AA**, and thus leads to similar sigmoidal kinetics as well.

The results here suggest that molecular packing can be used not just to optimize the static properties of the crystalline solid (elastic modulus, conductivity) but also its dynamic behavior. This could be useful for designing stimuli-responsive materials. For example, in photomechanical crystals, the deformation is proportional to the fraction of reacted molecules. Crystals like **9MA** and **9AcA**, in which the molecules are pre-positioned for photodimerization, will change shape uniformly during the illumination. **9CA** and **9AcA** crystals, on the other hand, will require an induction period before such shape changes can occur because the build-up of product molecules requires more time. This type of delayed response could be useful to reduce the sensitivity to stray light or provide a photonic threshold for a photomechanical shape change. On the other hand, if we desire the photomechanical response to be strictly proportional to the photon dose, **9MA** and **9AcA** might be better candidates.

Our correlation of nonclassical kinetics and spatially heterogeneous reaction progress suggests several future research directions. First, it would be interesting to examine in greater detail what kind of molecular conformational changes give rise to the heterogeneous photochemical reaction progress. This would require investigating other types of photoresponsive molecular single crystals to determine the generality of this phenomenon. Eventually, we would like to develop a theoretical model capable of predicting both how the quantum yield evolves during the reaction and how this evolution gives rise to the heterogeneous reaction dynamics.

Conclusions

In this study, we compared and evaluated the reaction progress on the optical length scale and the photochemical reaction kinetics on the molecular scale in single crystals of four anthracene derivatives with different substituents at the 9-position. From the changes in birefringence of single crystals upon photoirradiation, it was confirmed that in **9MA** and **9AcA**, the photochemical reaction takes place homogeneously throughout the crystal, but in **9AA** and **9CA**, the photochemical reaction propagates from the edges to the center. Furthermore, the change in absorbance *versus* irradiation time showed different sigmoidal curves depending on the compound. Quantitative analysis of the absorbance decay profiles revealed that **9AA** and **9CA** have a more pronounced cooperativity in the

photoreaction than those of **9AcA** and **9MA**. These results can be attributed to differences in the degree of molecular conformational and packing changes required for photodimerization. Namely, when the photodimerization reaction does not require large molecular packing changes (**9MA** and **9AcA**), the photochemical reaction proceeds homogeneously throughout the crystal on the optical length scale and the photochemical reaction kinetics are close to first-order (exponential). In contrast, when the photodimerization reaction requires large molecular packing changes (**9CA** and **9AA**), the photochemical reaction proceeds heterogeneously on the optical length scale (*i.e.*, the photochemical reaction propagates from the edge toward the center of the crystal). This is due to the high reactivity at the crystal surface and the high cooperativity required for the photochemical reaction. Going forward, it will be important to determine what fraction of solid-state reactions support spatially heterogeneous reaction kinetics, because they may give rise to qualitatively new behavior. For example, our results suggest that it may be possible to design materials exhibiting desired functions at arbitrary timings after a stimulus is applied.

Data availability

The data supporting this article have been included as part of the ESI.†

Author contributions

Sogo Kataoka: investigation, formal analysis, visualization, writing – original draft; Daichi Kitagawa: conceptualization, methodology, formal analysis, project administration, resources, supervision, writing – original draft, writing – review & editing; Hikaru Sotome: formal analysis, writing – review & editing; Syoji Ito: formal analysis, writing – review & editing; Hiroshi Miyasaka: formal analysis, writing – review & editing; Christopher J. Bardeen: formal analysis, project administration, writing – review & editing; Seiya Kobatake: resources, project administration, supervision, writing – review & editing.

Conflicts of interest

There are no conflicts to declare.

Acknowledgements

This work was partly supported by JSPS KAKENHI Grant Numbers JP21K14603, JP23H01926 (D. K.), JP21H01888, JP23H03956, JP23H04877 (H. S.), JP21KK0092, JP22K19007 (S. I.), JP21H01889, JP21K18934 (H. M.), JP21H02016 (S. K.) and the U.S. National Science Foundation DMR-1810514 (C. J. B.).

Notes and references

1 S. P. Anthony, *ChemPlusChem*, 2012, **77**, 518–531.
2 S.-J. Yoon, J. W. Chung, J. Gierschner, K. S. Kim, M.-G. Choi, D. Kim and S. Y. Park, *J. Am. Chem. Soc.*, 2010, **132**, 13675–13683.
3 S. Takamizawa and Y. Miyamoto, *Angew. Chem., Int. Ed.*, 2014, **53**, 6970–6973.
4 S. Takamizawa, Y. Takasaki, T. Sasaki and N. Ozaki, *Nat. Commun.*, 2018, **9**, 3984.
5 G. Liu, J. Liu, X. Ye, L. Nie, P. Gu, X. Tao and Q. Zhang, *Angew. Chem., Int. Ed.*, 2017, **56**, 198–202.
6 P. Commins, H. Hara and P. Naumov, *Angew. Chem., Int. Ed.*, 2016, **55**, 13028–13032.
7 S. Bhunia, S. Chandel, S. K. Karan, S. Dey, A. Tiwari, S. Das, N. Kumar, R. Chowdhury, S. Mondal, I. Ghosh, A. Mondal, B. B. Khatua, N. Ghosh and C. M. Reddy, *Science*, 2021, **373**, 321–327.
8 S. Mondal, P. Tanari, S. Roy, S. Bhunia, R. Chowdhury, A. K. Pal, A. Datta, B. Pal and C. M. Reddy, *Nat. Commun.*, 2023, **14**, 6589.
9 K. J. Msayib, D. Book, P. M. Budd, N. Chaukura, K. D. M. Harris, M. Helliwell, S. Tedds, A. Walton, J. E. Warren, M. Xu and N. B. McKeown, *Angew. Chem., Int. Ed.*, 2009, **48**, 3273–3277.
10 P. Naumov, S. Chizhik, M. K. Panda, N. K. Nath and E. Boldyreva, *Chem. Rev.*, 2015, **115**, 12440–12490.
11 W. M. Awad, D. W. Davies, D. Kitagawa, J. M. Halabi, M. B. Al-Handawi, I. Tahir, F. Tong, G. C. Alvarado, A. G. Shtukenberg, T. Alkhidir, Y. Hagiwara, M. Almehairbi, L. Lan, S. Hasebe, D. P. Karothu, S. Mohamed, H. Koshima, S. Kobatake, Y. Diao, R. Chandrasekar, H. Zhang, C. C. Sun, C. Bardeen, R. O. Al-Kaysi, B. Kahr and P. Naumov, *Chem. Soc. Rev.*, 2023, **52**, 3098–3169.
12 Z. M. Png, C.-G. Wang, J. C. C. Yeo, J. J. C. Lee, N. E. Surat'man, Y. L. Tan, H. Liu, P. Wang, B. H. Tan, J. W. Xu, X. J. Loh and Q. Zhu, *Mol. Syst. Des. Eng.*, 2023, **8**, 1097–1129.
13 Y. Ma, A. Zhang, X. Xue, D. Jiang, Y. Zhu and C. Zhang, *Cryst. Growth Des.*, 2014, **14**, 6101–6114.
14 M. Khalid, R. S. Ullah, M. A. Choudhary, M. N. Tahir, S. Murtaza, M. Hussain, B. Ali and Z. Ahmed, *J. Mol. Struct.*, 2018, **1167**, 57–68.
15 S. Kobatake, S. Takami, H. Muto, T. Ishikawa and M. Irie, *Nature*, 2007, **446**, 778–781.
16 H. Koshima, K. Takechi, H. Uchimoto, M. Shiro and D. Hashizume, *Chem. Commun.*, 2011, **47**, 11423–11425.
17 O. S. Bushuyev, A. Tomberg, T. Friščić and C. J. Barrett, *J. Am. Chem. Soc.*, 2013, **135**, 12556–12559.
18 T. Asahi, M. Suzuki and H. Masuhara, *J. Phys. Chem. A*, 2002, **106**, 2335–2340.
19 J. M. McBride, B. E. Segmuller, M. D. Hollingsworth, D. E. Mills and B. A. Weber, *Science*, 1986, **234**, 830–835.
20 N. M. Peachey and C. J. Eckhardt, *J. Am. Chem. Soc.*, 1993, **115**, 3519–3526.
21 I. Turowska-Tyrk, *J. Phys. Org. Chem.*, 2004, **17**, 837–847.
22 L. Bentea, M. A. Watzky and R. G. Finke, *J. Phys. Chem. C*, 2017, **121**, 5302–5312.

23 J. B. Benedict and P. Coppens, *J. Phys. Chem. A*, 2009, **113**, 3116–3120.
24 K. Morimoto, D. Kitagawa, F. Tong, K. Chalek, L. J. Mueller, C. J. Bardeen and S. Kobatake, *Angew. Chem., Int. Ed.*, 2022, **61**, e202114089.
25 K. Morimoto, D. Kitagawa, H. Sotome, S. Ito, H. Miyasaka and S. Kobatake, *Angew. Chem., Int. Ed.*, 2022, **61**, e202212290.
26 L. Li, P. Commins, M. B. Al-Handawi, D. P. Karothu, J. M. Halabi, S. Schramm, J. Weston, R. Rezgui and P. Naumov, *Chem. Sci.*, 2019, **10**, 7327–7332.
27 A. Khalil, D. P. Karothu and P. Naumov, *J. Am. Chem. Soc.*, 2019, **141**, 3371–3375.
28 H. Chung, D. Dudenko, F. Zhang, G. D'Avino, C. Ruzie, A. Richard, G. Schweicher, J. Cornil, D. Beljonne, Y. Geerts and Y. Diao, *Nat. Commun.*, 2018, **9**, 278.
29 D. W. Davies, B. Seo, S. K. Park, S. B. Shiring, H. Chung, P. Kafle, D. Yuan, J. W. Strzalka, R. Weber, X. Zhu, B. M. Savoie and Y. Diao, *Nat. Commun.*, 2023, **14**, 1304.
30 J. C. J. Bart and G. M. J. Schmidt, *Isr. J. Chem.*, 1971, **9**, 429–448.
31 K. Anderson, H. Becker, L. M. Engelhardt, L. Hansen and A. H. White, *Aust. J. Chem.*, 1984, **37**, 1337–1340.
32 H. Rabaud and J. Clastre, *Acta Crystallogr.*, 1959, **12**, 911–915.
33 J. Trotter, *Acta Crystallogr.*, 1959, **12**, 922–928.
34 K. Morimoto, H. Tsujioka, D. Kitagawa and S. Kobatake, *J. Phys. Chem. A*, 2020, **124**, 4732–4741.
35 K. Morimoto, H. Tsujioka, D. Kitagawa and S. Kobatake, *Bull. Chem. Soc. Jpn.*, 2019, **92**, 1299–1304.
36 A. S. Dvornikov and P. M. Rentzepis, *Res. Chem. Intermed.*, 1996, **22**, 115–128.
37 M. Bertmer, R. C. Nieuwendaal, A. B. Barnes and S. E. Hayes, *J. Phys. Chem. B*, 2006, **110**, 6270–6273.
38 R. S. Bogadi, D. C. Levendis and N. J. Coville, *J. Am. Chem. Soc.*, 2002, **124**, 1104–1110.
39 R. Destro, E. Ortoleva, R. Soave, L. Loconte and L. Lo Presti, *Phys. Chem. Chem. Phys.*, 2009, **11**, 7181–7188.
40 P. Naumov, P. Makreski, G. Petruševski, T. Runčevski and G. Jovanovski, *J. Am. Chem. Soc.*, 2010, **132**, 11398–11401.
41 T. Salzillo, S. Zaccheroni, R. G. Della Valle, E. Venuti and A. Brillante, *J. Phys. Chem. C*, 2014, **118**, 9628–9635.
42 F. Tong, M. P. Hanson and C. J. Bardeen, *Phys. Chem. Chem. Phys.*, 2016, **18**, 31936–31945.
43 W. Urbach, H. Hervet and F. Rondelez, *Mol. Cryst. Liq. Cryst.*, 1978, **46**, 209–221.
44 I. Zouev, T. Lavy and M. Kaftory, *Eur. J. Org Chem.*, 2006, **18**, 4164–4169.
45 C. R. Theocharis and W. Jones, *J. Chem. Soc., Faraday Trans.*, 1985, **1**(81), 857–874.
46 M. Ehrenberg, *Acta Crystallogr., Sect. B: Struct. Crystallogr. Cryst. Chem.*, 1968, **24**, 1123–1125.
47 D. Craig and P. Sarti-Fantoni, *Chem. Commun.*, 1966, 742–743.
48 A. Kawada and M. M. Labes, *Mol. Cryst. Liq. Cryst.*, 1970, **11**, 133–144.